

# Three-dimensional Fermi surfaces from charge order in layered $\text{CsV}_3\text{Sb}_5$

Xiangwei Huang<sup>1</sup>, Chunyu Guo<sup>1,2,\*</sup>, Carsten Putzke<sup>1,2</sup>, Martin Gutierrez-Amigo<sup>3,4</sup>, Yan Sun,<sup>5</sup> Maia G. Vergniory,<sup>5,6</sup> Ion Errea,<sup>4,6,7</sup> Dong Chen<sup>5</sup>, Claudia Felser,<sup>5</sup> and Philip J. W. Moll<sup>1,2,†</sup>

<sup>1</sup>Laboratory of Quantum Materials (QMAT), Institute of Materials (IMX), École Polytechnique Fédérale de Lausanne (EPFL), CH-1015 Lausanne, Switzerland

<sup>2</sup>Max Planck Institute for the Structure and Dynamics of Matter, 22761 Hamburg, Germany


<sup>3</sup>Department of Physics, University of the Basque Country (UPV/EHU), 48080 Bilbao, Spain

<sup>4</sup>Centro de Física de Materiales (CSIC-UPV/EHU), 20018 Donostia-San Sebastian, Spain

<sup>5</sup>Max Planck Institute for Chemical Physics of Solids, 01187 Dresden, Germany

<sup>6</sup>Donostia International Physics Center, 20018 Donostia-San Sebastian, Spain

<sup>7</sup>Fisika Aplikatua Saila, Gipuzkoako Ingeniaritza Eskola, University of the Basque Country (UPV/EHU), 20018 Donostia-San Sebastian, Spain

 (Received 17 January 2022; revised 4 August 2022; accepted 8 August 2022; published 23 August 2022)

The cascade of electronic phases in  $\text{CsV}_3\text{Sb}_5$  raises the prospect to disentangle their mutual interactions in a clean, strongly interacting kagome lattice. When the kagome planes are stacked into a crystal, its electronic dimensionality encodes how much of the kagome physics and its topological aspects survive. The layered structure of  $\text{CsV}_3\text{Sb}_5$  reflects in Brillouin-zone-sized quasi-two-dimensional Fermi surfaces and significant transport anisotropy. Yet here we demonstrate that  $\text{CsV}_3\text{Sb}_5$  is a three-dimensional (3D) metal within the charge density wave (CDW) state. Small 3D pockets play a crucial role in its low-temperature magneto- and quantum transport. Their emergence at  $T_{\text{CDW}} \approx 93$  K results in an anomalous sudden increase of the in-plane magnetoresistance by four orders of magnitude. The presence of these 3D pockets is further confirmed by quantum oscillations under in-plane magnetic fields, demonstrating their closed nature. These results emphasize the impact of interlayer coupling on the kagome physics in 3D materials.

DOI: [10.1103/PhysRevB.106.064510](https://doi.org/10.1103/PhysRevB.106.064510)

## I. INTRODUCTION

When structurally layered materials host strong electronic correlations, their effective electronic dimensionality is key to understanding their microscopic physics. The anisotropic Fermi surface then sets the canvas on which correlated ground states unfold, such as magnetism, charge density waves (CDW), or superconductivity. Cuprate and pnictide high-temperature superconductors are prime examples of layered materials in which reduced dimensionality defines the superconducting state [1,2]. The anisotropy is further a critical parameter to describe the vortex formation and the orbital limit of the upper critical field. Recently, metals hosting planes with kagome nets have attracted significant attention due to their topological phases as well as potential correlation effects [3–5]. The latter have been argued to arise from small-bandwidth bands (flat bands) that are predicted in phenotypical two-dimensional (2D) kagome models [6]. Flat bands naturally enhance correlation effects when the Coulomb energy exceeds the kinetic energy and they lead to a divergent density of states, an entropic catastrophe which is commonly avoided by the formation of electronically ordered states at low temperatures. However, when the kagome nets are stacked

into a three-dimensional (3D) crystal, the existence of flat bands depends on the strength of the interlayer hybridization and its impact on band dispersion. Therefore, in order to explore how much kagome physics survives in a 3D metal, it is necessary to investigate the electronic structure and especially its effective dimensionality.

Here we investigate the electronic dimensionality of  $\text{CsV}_3\text{Sb}_5$  [Figs. 1(a) and 1(b)], a stacked kagome crystal, and its influence on the rich physics it hosts, such as the nontrivial band topology, superconductivity, and CDW order. The nonmagnetic kagome nets formed by vanadium atoms result in a symmetry-enforced pair of  $\mathbb{Z}_2$  topological bands with opposite Chern numbers [5,7–9]. The hybridization with Sb atoms effectively expands the bandwidth, and therefore the flat band gains sizable dispersion yet leaves multiple bulk Dirac points intact, as observed by angle-resolved photoemission spectroscopy (ARPES) [7,10]. Upon cooling, the kagome lattice undergoes a CDW transition at  $T_{\text{CDW}} = 93$  K [11–13]. The  $2 \times 2$  reconstruction within the kagome plane is accompanied by a  $\pi$  phase shift of the CDW across an atomic step edge as observed by STM experiments [13,14], suggesting a band reconstruction along the  $c$  direction. X-ray studies further suggest a  $2 \times 2 \times 4$  superlattice formation [15,16] with long-range out-of-plane coherence, again highlighting the importance of out-of-plane coupling in this system. At even lower temperatures of  $T_c \approx 2.8$  K, superconductivity appears [7]. The large upper critical field anisotropy ( $\sim 9$ ) is a result of

\*chunyu.guo@mpsd.mpg.de

†philip.moll@mpsd.mpg.de

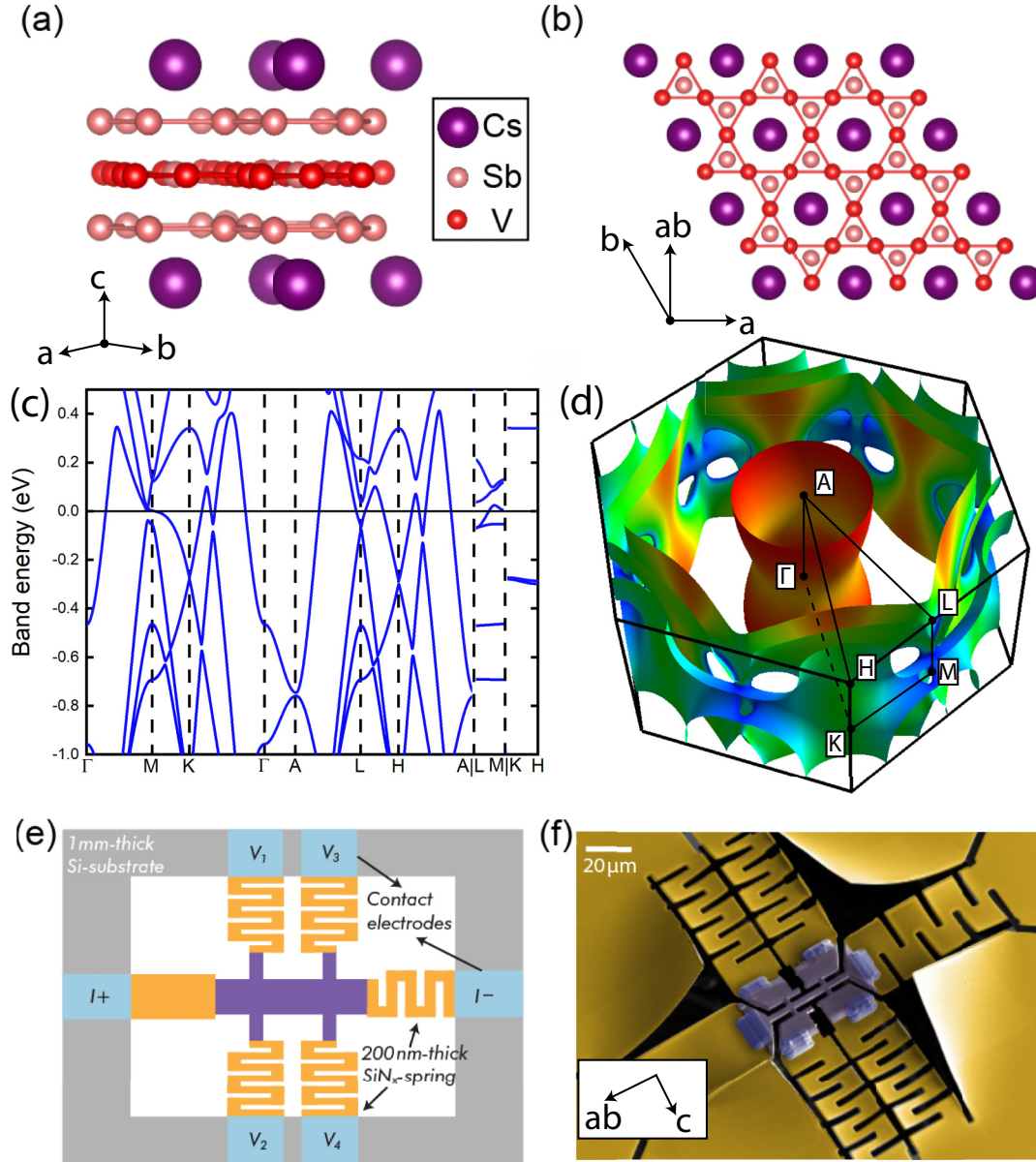


FIG. 1. (a) Side and (b) top view of crystal structure of  $\text{CsV}_3\text{Sb}_5$ , which consists of layers of Cs, V, and Sb atoms that form the kagome lattice plane. (c) Electronic structure of  $\text{CsV}_3\text{Sb}_5$  calculated by density-functional theory. There exist multiple electronic bands across the Fermi level. (d) Fermi surfaces in the Brillouin zone, including several types of Fermi surfaces and their symmetric copies. (e) Illustration of membrane-mount  $\text{CsV}_3\text{Sb}_5$  device. The sample is suspended with soft  $\text{SiN}_x$  springs, which ensures minimum strain effect. (f) Scanning electron microscope (SEM) image of the membrane device. The  $250 \times 250 \mu\text{m}$  membrane window was patterned into several branches of springs with FIB.

its anisotropic superconducting properties [17]. Meanwhile, the nontrivial band topology may give rise to topological superconductivity. Indeed, STM has uncovered a zero-bias peak in the vortex cores which, while not conclusive, is compatible with a scenario of bound Majorana states [13].

## II. RESULTS

The single-particle band structure from *ab initio* calculations serves as a starting point to investigate the dimensionality of this strongly correlated compound. The electronic structure of  $\text{CsV}_3\text{Sb}_5$  in the high-symmetry state at room tem-

perature is calculated using density functional theory (DFT) methods, and the computational details can be found in the Supplemental Material [18] (see also Refs. [19–23]). Multiple bands are found at the Fermi level [Fig. 1(c)], consistent with the previous reports [5,7,8]. Accordingly, multiple Fermi surfaces of cylindrical shape are expected in the Brillouin zone [Fig. 1(d)]. While the layered structure is reflected in the electroniclike cylinders centered at  $\Gamma$  and K, their sizable dispersion signals pronounced interlayer coupling. In absence of spin-orbit coupling (SOC), the cylinder at the Brillouin zone boundary (H to K) would surround a nodal line, yet SOC breaks this degeneracy gapping the nodal line.

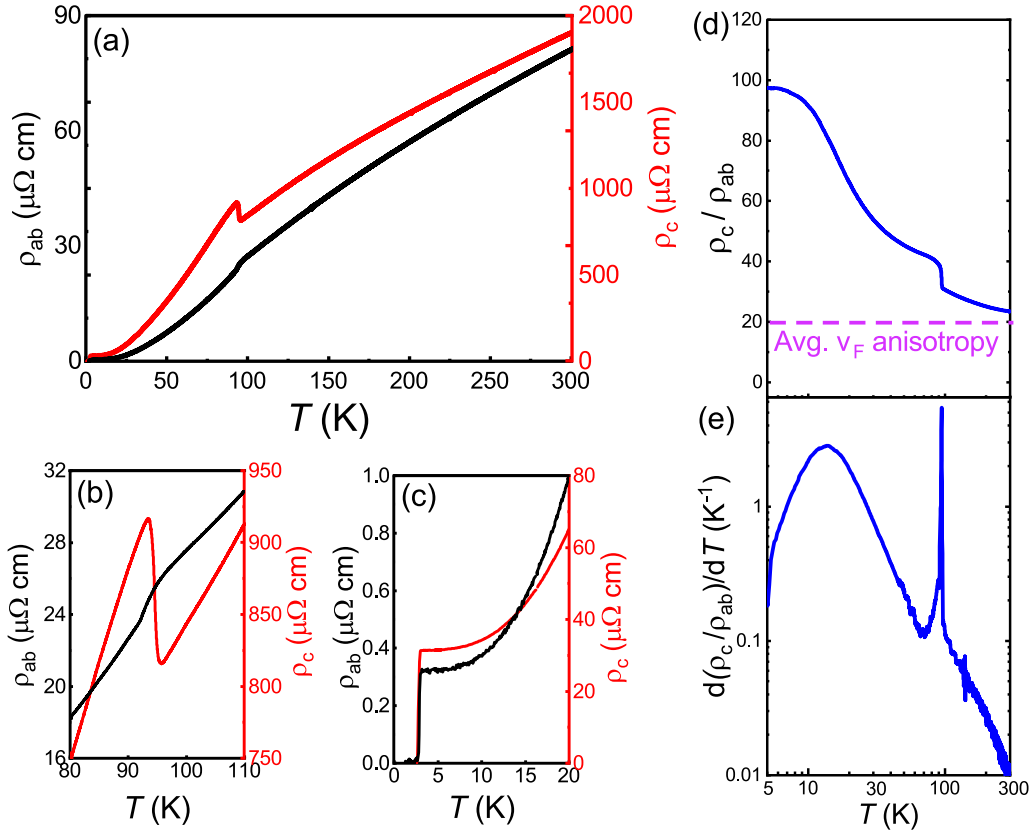


FIG. 2. (a) Temperature dependence of the out-of-plane ( $\rho_c$ ) and in-plane resistivity ( $\rho_{ab}$ ). (b) An abrupt jump occurs in the temperature dependence of  $\rho_c$ , which corresponds to the charge-density-wave transition temperature  $T_{CDW}$ . Consistently,  $\rho_{ab}$  also displays a weak discontinuity. (c) Enlarged view of (a) within the low-temperature range which demonstrates a clear superconducting transition at  $T_c = 2.8$  K. (d) Temperature dependence of resistivity anisotropy ( $\rho_c/\rho_{ab}$ ). The dashed lines stand for the averaged Fermi velocity anisotropy for all Fermi surfaces. (e) First-order derivative of temperature dependence of resistivity anisotropy [ $d(\rho_c/\rho_{ab})/dT$ ]. At the charge-density-wave transition temperature ( $T_{CDW}$ ) a sharp peak can be observed, as well as a broad hump at  $T'' \approx 14$  K.

The band structure of  $\text{CsV}_3\text{Sb}_5$  indicates a clear out-of-plane dispersion, giving rise to warping of the cylindrical Fermi surfaces. Experimentally the electronic dimensionality can be explored via resistivity anisotropy. As is common in structurally layered materials,  $\text{CsV}_3\text{Sb}_5$  crystals grow as thin platelets along the kagome plane [5]. While this crystal morphology lends itself to in-plane resistivity measurements, quantitative out-of-plane transport poses a well-known challenge. Focused ion beam (FIB) milling can be used to prepare micron-sized  $c$ -direction bars with well-defined geometries to quantify the resistivity [24].  $\text{CsV}_3\text{Sb}_5$ , like other soft CDW compounds, is susceptible to mechanical strain [25,26], so we suspend the microstructured sample (purple) in free space. It is mechanically and electrically connected to a supportive silicon frame only via thin, gold-coated  $\text{SiN}_x$  membrane microsprings (gold) [Figs. 1(e) and 1(f)]. These structures exert only minimal residual pressure on the sample ( $\sim 9.8$  bar, see Supplemental Material [18]), thus allowing an intrinsic evolution of the ordered states. Moreover, a low-voltage polish step at 5 kV reduces the amorphization layer into the nanometer range [27], which minimizes its possible influence.

In these suspended structures, the in-plane resistivity decreases from  $80 \mu\Omega \text{ cm}$  at 300 K to  $0.3 \mu\Omega \text{ cm}$  at  $T_c = 2.8$  K. The high residual resistivity ratio (RRR) of 250 is compara-

ble to bulk samples [9], evidencing the high quality of the microstructure fabrication (Fig. 2). The in-plane resistivity displays a small yet sharply defined discontinuity at the CDW transition at  $T_{CDW}$ , which is consistent with previous reports [5,9,28]. The out-of-plane resistivity  $\rho_c$  is comparably larger yet shows an overall similar metallic temperature dependence. It decreases from  $\rho_c(300 \text{ K}) \sim 1.9 \text{ m}\Omega \text{ cm}$  to  $\rho_c(T_c) \approx 33 \mu\Omega \text{ cm}$ , corresponding to a lower RRR of 60. These results are qualitatively reflected in the challenging measurements of  $\rho_c$  on bulk crystals [7,28], yet deviate quantitatively. In comparison to the in-plane resistivity,  $\rho_c$  shows an upward jump at  $T_{CDW}$  [Fig. 2(c)]. This jump of  $[\rho_c(T_{CDW}^-) - \rho_c(T_{CDW}^+)/\rho_c(T_{CDW}^+)] \approx 12\%$  is much more pronounced compared to the change of  $\sim -3\%$  for in-plane resistivity. This relative difference again emphasizes the importance of the CDW in the out-of-plane direction.

Further information about the electronic dimensionality is contained in the temperature dependence of the anisotropy. At high temperatures above  $T_{CDW}$ , the picture of an anisotropic metal emerges [ $\rho_c/\rho_{ab}(T = 300 \text{ K}) \approx 24$ ], which falls close to the Fermi velocity anisotropy when averaged over the entire Fermi surface ( $|v_{F,\parallel}|/|v_{F,\perp}| \approx 20$ , [Fig. 2(d)]). The dominant carrier density originates from the Brillouin-zone-sized hexagonal Fermi surfaces with weak  $k_z$  dispersion. These feature six almost-flat surfaces parallel to the crystalline  $a$

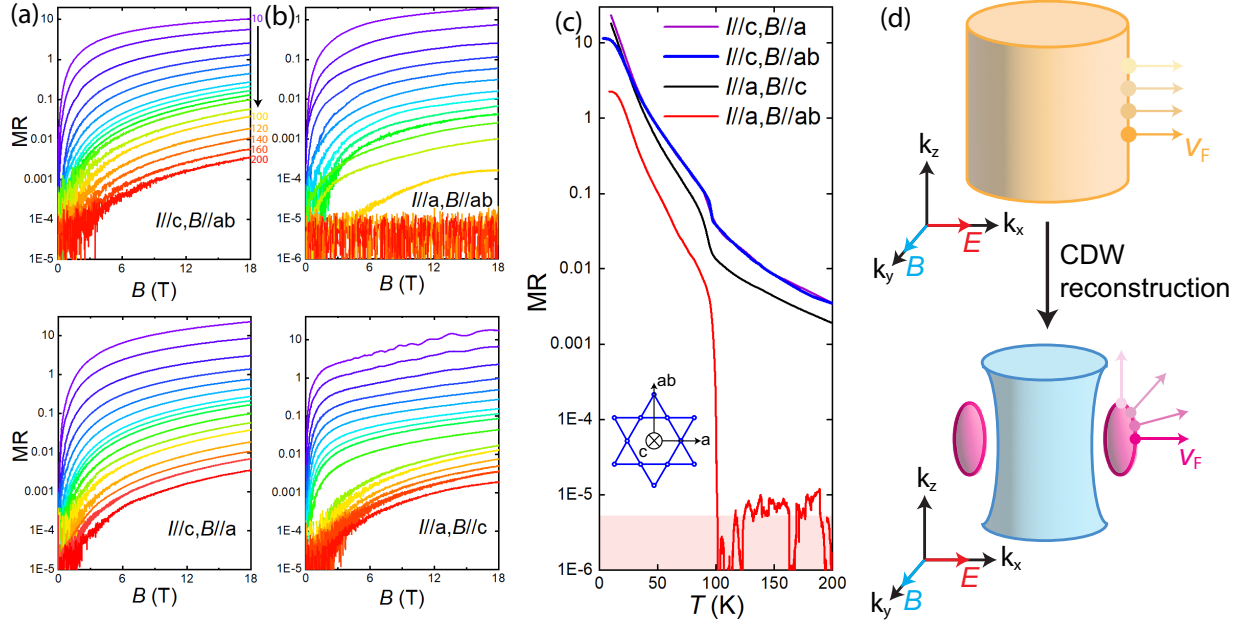


FIG. 3. Field dependence of (a) out-of-plane and (b) in-plane magnetoresistance ratio [ $MR = (\rho(18\text{ T}) - \rho(0\text{ T}))/\rho(0\text{ T})$ ] with field applied along the  $a$  and  $c(ab)$  axis. (c) Temperature dependence of magnetoresistance ratio at  $B = 18\text{ T}$  with current along the  $ab$  axis and field along the  $a$  axis, which are defined in the inset. (d) Illustration of Fermi surface reconstruction due to charge ordering. The abrupt appearance of magnetoresistance below  $T_{CDW}$  is a direct consequence of the 3D pockets that appear only after the CDW reconstruction.

directions [Fig. 1(b)], which play an important role in the magneto-transport as discussed later.

Further lowering the temperature beyond the jump at  $T_{CDW}$  increases the anisotropy, which eventually saturates around 100 at  $T_c$ , suggesting dominant in-plane electronic transport at low temperatures. Yet  $\rho_c$  reaches a low value of  $33\ \mu\Omega\text{ cm}$  at  $T_c$ , which signals metallic three-dimensional transport. The first-order derivative of the resistivity anisotropy reveals further, more subtle changes in the material [Fig. 2(e)]. Besides the clear spike at  $T_{CDW}$ , a local minimum occurs at around 70 K. This temperature coincides with the onset of anisotropy in the muon spin depolarization rate that has been associated with time-reversal-symmetry breaking (TRSB) [29]. The TRSB state has been theoretically proposed to arise from an effective orbital current loop flux [30,31], and a modification of a magnetic scattering channel would be a natural connection between this experiment and ours.

This further emphasizes the emerging question about its effective electronic dimensionality. The large resistivity anisotropy is compatible with an effective 2D description, which may be captured by a simplified model based on a 2D kagome lattice. Yet to discuss the effective dimensionality, one has to carefully distinguish between the transport dimensionality and the dimensionality of the Fermi surface. In general, the transport anisotropy is determined by the Fermi velocity  $v_F(k)$  and the scattering time  $\tau(k)$  distribution, while the Fermi surface topology encodes another aspect of electronic dimensionality. For example, a cylindrical Fermi surface with strong warping naturally features low transport anisotropy. Here we demonstrate that  $\text{CsV}_3\text{Sb}_5$  is a 3D kagome metal as the emergent small, closed Fermi pockets play a crucial role in its magneto- and quantum transport properties.

The magnetoresistance provides further information about the electronic dimensionality (Fig. 3). Most intriguing is the complete absence of transverse magnetoresistance for orthogonal in-plane fields and currents at any temperature above  $T_{CDW}$ . The field-independent noise floor provides an upper bound for the magnetoresistance, at  $\Delta\rho_a(18\text{ T})/\rho_a(0\text{ T}) < 10^{-5}$  at 120 K, here  $\delta\rho_a = \rho_a(18\text{ T}) - \rho_a(0\text{ T})$ . Even rather unassuming metals such as Cu commonly show transverse magnetoresistance around 1% (20 T) at room temperature and 100% (20 T) at 100 K [32]. In contrast, for all other orthogonal current and field orientations in  $\text{CsV}_3\text{Sb}_5$ , the magnetoresistance increases with decreasing temperature following a conventional semiclassical scaling of the magneto-transport by  $\omega_c\tau$ . Given the complex Fermi surface and putative incipient TRSB order, such absent magnetoresistance for one particular direction appears quite exotic.

The reconstruction of the main cylindrical Fermi surfaces at  $T_{CDW}$  offers a natural explanation for such behavior. When a current is applied in the plane, the conductivity is dominated by the weakly warped main Fermi surfaces [Fig. 3(d)]. Such flatness ensures that the quasiparticle velocity remains approximately unchanged by the Lorentz force. This behavior is commonly observed in quasi-2D materials when only cylindrical Fermi surfaces are present [33,34]. For magnetic field or current applied along any other direction, magnetoresistance is bound to appear as the Lorentz force significantly impacts the carrier trajectories. These results consistently demonstrate that  $\text{CsV}_3\text{Sb}_5$  is electronically quasi-2D above  $T_{CDW}$ .

However, this conclusion no longer holds in the charge ordered phase. Though the exact type of CDW reconstruction is still under debate, all different scenarios predict the emergence of small closed 3D pockets as a direct consequence of zone folding [35]. Compared to the quasi-2D Fermi

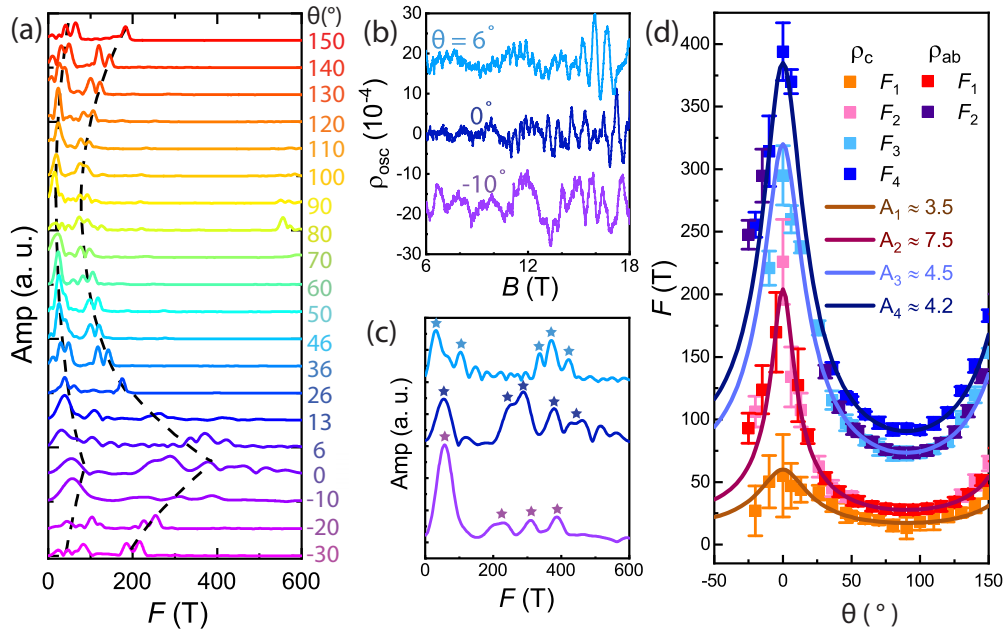


FIG. 4. (a) Fast-Fourier-transformation (FFT) spectrum with different field directions for Shubnikov-de-Hass (SdH) oscillations measured with current applied along the  $c$  axis. Here  $\theta$  stands for the angle between the  $a$  axis and field direction. (b) SdH oscillations ( $\rho_{\text{osc}}$ ) at  $\theta = 6^\circ$ ,  $0^\circ$ , and  $-10^\circ$ . Here  $\rho_{\text{osc}} = \Delta\rho/\rho_{BG}$ , with  $\Delta\rho$  as the oscillatory part of the magnetoresistivity and  $\rho_{BG}$  as a polynomial fit to the magnetoresistivity background. (c) Corresponding FFT spectrum with star symbols indicating the identified peaks. (d) Angular dependence of SdH oscillation frequencies. The error bar is defined as full width at half maximum of the peaks in the FFT spectrum.

surfaces, these small pockets support closed cyclotron orbits which lead to the sudden recovery of magnetoresistance [Fig. 3(d)]. The direct connection between the abrupt change of magnetoresistance and Fermi surface reconstruction further demonstrates the importance of the small, closed pockets to the 3D electronic transport properties of  $\text{CsV}_3\text{Sb}_5$ , especially at low temperatures.

Such small 3D-like pockets at low temperature should be visible in quantum oscillations. Four low-frequency quantum oscillations have been reported for out-of-plane fields and associated with these small 3D pockets [11,35]. However, these quantum oscillations were observed to quickly disappear as the field is rotated toward the plane, which precluded the distinction between a closed 3D pocket and an open 2D cylinder. The weakly perturbed, suspended microbars now allow to track this frequency over the entire angle range, firmly establishing them as closed 3D pockets within the density wave phase (Fig. 4). At low angles, the oscillation frequencies observed in our structures are consistent with these previous reports. A likely scenario for the loss of amplitude in conventional experiments involves stacking disorder along the  $c$  direction due to residual strain, which reduces the quantum-coherent transport along the out-of-plane direction. This is consistent with the larger RRR and lower resistivity observed in the microstructures compared to macroscopic crystals [7,28]. The angular dependence of the oscillation frequencies is well described by a simple ellipsoidal model  $F_i \propto 1/\sqrt{\sin^2(\theta) + (1 + A_i^2)\cos^2(\theta)}$ . The factor  $A_i$  characterizes the anisotropy of the  $i$ th Fermi surface [Fig. 4(d)]. These results further support the presence of 3D pockets as suggested by the unusual magneto-transport.

The emergence of 3D Fermi pockets due to CDW reconstruction has already been observed in other CDW materials [36,37], as a 3D zone-folding of Brillouin-zone-sized Fermi surface naturally results in small Fermi surface pockets. These pockets are connected by the  $3/4$  Bragg wave vector in the 3Q directions, which results in an exotic pairing density wave phase at low temperature [38], as observed in STM experiments [39]. Here 3Q stands for the triple  $q$ -wavevector for the charge density wave.

In conclusion, the electronic anisotropy and Fermiology of charge-ordered  $\text{CsV}_3\text{Sb}_5$  are characterized by the coexistence of a high-mobility in-plane electronic system with small 3D pockets. They emerge when the charge order is established, demonstrating an electronic dimensionality crossover at  $T_{\text{CDW}}$ . Therefore, the interlayer coupling must be taken into account for theoretical modeling as considerations based on 2D kagome lattices may miss important aspects of this material. It will be highly interesting to explore how the cascades of correlated electronic states are influenced by the coupling between kagome nets.

## ACKNOWLEDGMENTS

This work was funded by the European Research Council (ERC) under the European Union's Horizon 2020 Research and Innovation program (MiTopMat, Grant No. 715730). This project received funding from the Swiss National Science Foundation (Grant No. PP00P2\_176789). M.G.V., I.E., and M.G.A. acknowledge the Spanish Ministerio de Ciencia e Innovación (Grant No. PID2019-109905GB-C21). M.G.V. acknowledges support from Programa Red Guipuzcoana de Ciencia Tecnología e Innovación 2021, No.

2021-CIEN-000070-01 Gipuzkoa Next, and the Deutsche Forschungsgemeinschaft (DFG, German Research Foundation) through GA 3314/1-1-FOR 5249 (QUAST). This work has been supported in part by the Basque Government (Grant No. IT979-16). This work was also supported by the European Research Council (Advanced Grant No. 742068

TOPMAT), the Deutsche Forschungsgemeinschaft (Project ID No. 258499086 SFB 1143), and the DFG through the Würzburg-Dresden Cluster of Excellence on Complexity and Topology in Quantum Matter ct.qmat (EXC 2147, Project ID No. 39085490). The authors declare that they have no competing financial interests.

- [1] J. G. Bednorz and K. A. Müller, *Z. Phys. B: Condens. Matter* **64**, 189 (1986).
- [2] Y. Kamihara, H. Hiramatsu, M. Hirano, R. Kawamura, H. Yanagi, T. Kamiya, and H. Hosono, *J. Am. Chem. Soc.* **128**, 10012 (2006).
- [3] T. Kida, L. Fenner, A. Dee, I. Terasaki, M. Hagiwara, and A. Wills, *J. Phys.: Condens. Matter* **23**, 112205 (2011).
- [4] M. Kang, S. Fang, L. Ye, H. C. Po, J. Denlinger, C. Jozwiak, A. Bostwick, E. Rotenberg, E. Kaxiras, J. G. Checkelsky *et al.*, *Nat. Commun.* **11**, 4004 (2020).
- [5] B. R. Ortiz, L. C. Gomes, J. R. Morey, M. Winiarski, M. Bordelon, J. S. Mangum, I. W. H. Oswald, J. A. Rodriguez-Rivera, J. R. Neilson, S. D. Wilson, E. Ertekin, T. M. McQueen, and E. S. Toberer, *Phys. Rev. Materials* **3**, 094407 (2019).
- [6] A. O'Brien, F. Pollmann, and P. Fulde, *Phys. Rev. B* **81**, 235115 (2010).
- [7] B. R. Ortiz, S. M. L. Teicher, Y. Hu, J. L. Zuo, P. M. Sarte, E. C. Schueller, A. M. Milinda Abeykoon, M. J. Krogstad, S. Rosenkranz, R. Osborn, R. Seshadri, L. Balents, J. He, and S. D. Wilson, *Phys. Rev. Lett.* **125**, 247002 (2020).
- [8] Y. Fu, N. Zhao, Z. Chen, Q. Yin, Z. Tu, C. Gong, C. Xi, X. Zhu, Y. Sun, K. Liu, and H. Lei, *Phys. Rev. Lett.* **127**, 207002 (2021).
- [9] D. Chen, B. He, M. Yao, Y. Pan, H. Lin, W. Schnelle, Y. Sun, J. Gooth, L. Taillefer, and C. Felser, *Phys. Rev. B* **105**, L201109 (2022).
- [10] Y. Luo, S. Peng, S. M. Teicher, L. Huai, Y. Hu, B. R. Ortiz, Z. Wei, J. Shen, Z. Ou, B. Wang *et al.*, *arXiv:2106.01248* (2021).
- [11] F. H. Yu, T. Wu, Z. Y. Wang, B. Lei, W. Z. Zhuo, J. J. Ying, and X. H. Chen, *Phys. Rev. B* **104**, L041103 (2021).
- [12] C. Mu, Q. Yin, Z. Tu, C. Gong, H. Lei, Z. Li, and J. Luo, *Chin. Phys. Lett.* **38**, 077402 (2021).
- [13] Z. Liang, X. Hou, F. Zhang, W. Ma, P. Wu, Z. Zhang, F. Yu, J.-J. Ying, K. Jiang, L. Shan *et al.*, *Phys. Rev. X* **11**, 031026 (2021).
- [14] H. Zhao, H. Li, B. R. Ortiz, S. M. Teicher, T. Park, M. Ye, Z. Wang, L. Balents, S. D. Wilson, and I. Zeljkovic, *Nature (London)* **599**, 216 (2021).
- [15] S. Wu, B. R. Ortiz, H. Tan, S. D. Wilson, B. Yan, T. Birol, and G. Blumberg, *Phys. Rev. B* **105**, 155106 (2022).
- [16] Q. Stahl, D. Chen, T. Ritschel, C. Shekhar, E. Sadrollahi, M. C. Rahn, O. Ivashko, M. v. Zimmermann, C. Felser, and J. Geck, *Phys. Rev. B* **105**, 195136 (2022).
- [17] S. Ni, S. Ma, Y. Zhang, J. Yuan, H. Yang, Z. Lu, N. Wang, J. Sun, Z. Zhao, D. Li *et al.*, *Chin. Phys. Lett.* **38**, 057403 (2021).
- [18] See Supplemental Material at <http://link.aps.org/supplemental/10.1103/PhysRevB.106.064510> for a description of the fabrication process of the MEM-based microstructures, an estimation of strain due to thermal contraction for MEM-based microstructure, and the details of band structure calculations.
- [19] P. Giannozzi, Jr., O. Andreussi, T. Brumme, O. Bunau, M. B. Nardelli, M. Calandra, R. Car, C. Cavazzoni, D. Ceresoli, M. Cococcioni, N. Colonna, I. Carnimeo, A. D. Corso, S. de Gironcoli, P. Delugas, R. A. DiStasio, Jr., A. Ferretti, A. Floris, G. Fratesi, G. Fugallo *et al.*, *J. Phys.: Condens. Matter* **29**, 465901 (2017).
- [20] J. P. Perdew, K. Burke, and M. Ernzerhof, *Phys. Rev. Lett.* **77**, 3865 (1996).
- [21] A. Dal Corso, *Comput. Mater. Sci.* **95**, 337 (2014).
- [22] M. Methfessel and A. T. Paxton, *Phys. Rev. B* **40**, 3616 (1989).
- [23] A. A. Mostofi, J. R. Yates, G. Pizzi, Y.-S. Lee, I. Souza, D. Vanderbilt, and N. Marzari, *Comput. Phys. Commun.* **185**, 2309 (2014).
- [24] P. J. W. Moll, *Annu. Rev. Condens. Matter Phys.* **9**, 147 (2018).
- [25] B. Song, X. Kong, W. Xia, Q. Yin, C. Tu, C. Zhao, D. Dai, K. Meng, Z. Tao, Z. Tu *et al.*, *arXiv:2105.09248*.
- [26] F. Du, S. Luo, B. R. Ortiz, Y. Chen, W. Duan, D. Zhang, X. Lu, S. D. Wilson, Y. Song, and H. Yuan, *Phys. Rev. B* **103**, L220504 (2021).
- [27] R. Kelley, K. Song, B. Van Leer, D. Wall, and L. Kwakman, *Microsc. Microanal.* **19**, 862 (2013).
- [28] Y. Xiang, Q. Li, Y. Li, W. Xie, H. Yang, Z. Wang, Y. Yao, and H.-H. Wen, *Nat. Commun.* **12**, 6727 (2021).
- [29] L. Yu, C. Wang, Y. Zhang, M. Sander, S. Ni, Z. Lu, S. Ma, Z. Wang, Z. Zhao, H. Chen *et al.*, *arXiv:2107.10714*.
- [30] M. M. Denner, R. Thomale, and T. Neupert, *Phys. Rev. Lett.* **127**, 217601 (2021).
- [31] X. Feng, K. Jiang, Z. Wang, and J. Hu, *Sci. Bull.* **66**, 1384 (2021).
- [32] J. de Launay, R. Dolecek, and R. Webber, *J. Phys. Chem. Solids* **11**, 37 (1959).
- [33] B. Korin-Hamzić, M. Basletić, and K. Maki, *Europhys. Lett.* **59**, 298 (2002).
- [34] J. Wosnitza, *Fermi Surfaces of Low-Dimensional Organic Metals and Superconductors* (Springer, New York, 2006), Vol. 134.
- [35] B. R. Ortiz, S. M. L. Teicher, L. Kautzsch, P. M. Sarte, N. Ratcliff, J. Harter, J. P. C. Ruff, R. Seshadri, and S. D. Wilson, *Phys. Rev. X* **11**, 041030 (2021).
- [36] P. Knowles, B. Yang, T. Muramatsu, O. Moulding, J. Buhot, C. J. Sayers, E. Da Como, and S. Friedemann, *Phys. Rev. Lett.* **124**, 167602 (2020).
- [37] C. C. Tam, M. Zhu, J. Ayres, K. Kummer, F. Yakhov-Harris, J. R. Cooper, A. Carrington, and S. M. Hayden, *Nat. Commun.* **13**, 570 (2022).
- [38] S. Zhou and Z. Wang, *arXiv:2110.06266* (2021).
- [39] H. Chen, H. Yang, B. Hu, Z. Zhao, J. Yuan, Y. Xing, G. Qian, Z. Huang, G. Li, Y. Ye, S. Ma, S. Ni, H. Zhang, Q. Yin, C. Gong, Z. Tu, H. Lei, H. Tan, S. Zhou, C. Shen *et al.*, *Nature (London)* **599**, 222 (2021).